

DeepMech: A Machine Learning Framework for Chemical Reaction Mechanism Prediction

Manajit Das¹†, Ajnabiul Hoque¹†, Mayank Baranwal^{2,3*}, and Raghavan B. Sunoj^{1,4*}

¹Department of Chemistry, Indian Institute of Technology Bombay; Mumbai, 400076, India.

²Department of Systems and Control Engineering, Indian Institute of Technology Bombay; Mumbai, 400076, India.

³Tata Consultancy Services Research; Mumbai, India.

⁴Centre for Machine Intelligence and Data Science, Indian Institute of Technology Bombay; Mumbai, 400076, India.

*Corresponding authors. Emails: sunoj@chem.iitb.ac.in, mbaranwal@iitb.ac.in

†These authors contributed equally to this work.

Abstract

Prediction of complete step-by-step chemical reaction mechanisms (CRMs) remains a major challenge. Whereas the traditional approaches in CRM tasks rely on expert-driven experiments or costly quantum chemical computations, contemporary deep learning (DL) alternatives ignore key intermediates and mechanistic steps and often suffer from hallucinations. We present DeepMech, an interpretable graph-based DL framework employing atom- and bond-level attention, guided by generalized templates of mechanistic operations (TMOps), to generate CRMs. Trained on our curated ReactMech dataset (~30K CRMs with 100K atom-mapped and mass-balanced elementary steps), DeepMech achieves $98.98 \pm 0.12\%$ accuracy in predicting elementary steps and $95.94 \pm 0.21\%$ in complete CRM tasks, besides maintaining high fidelity even in out-of-distribution scenarios as well as in predicting side and/or byproducts. Extension to multistep CRMs relevant to prebiotic chemistry, demonstrates the ability of DeepMech in effectively reconstructing

pathways from simple primordial substrates to complex biomolecules such as serine and aldopentose. Attention analysis identifies reactive atoms/bonds in line with chemical intuition, rendering our model interpretable and suitable for reaction design.

Introduction

Chemical reactions form the foundation of synthesis of vital compounds such as drugs, pharmaceuticals, agrochemicals, etc., enabling the construction of complex molecules bearing tailored properties.¹ In a chemical reaction, reactants convert to products through one or more elementary steps (Fig. 1A). A meaningful description of such elementary steps and the associated intermediates in a reaction is referred to as reaction mechanism. A deeper understanding of chemical reaction mechanism (CRM) is indispensable in discovering new reactions and in designing molecules of high importance.² Heuristic methods, such as the arrow-pushing formalism, are traditionally used to rationalize reaction pathways.³ However, chemical intuition alone often remains inadequate for navigating newer and complex reaction pathways. The need for a reliable, robust, and fast computational method for CRM prediction is of great current interest.

Several attempts to design complete CRMs, centered on rather tedious quantum chemical computations, have been reported.^{4,5,6,7} Although such methods can offer valuable mechanistic insights (Fig. 1B), it involves high computational costs and are often confined to applications to small molecules (typically fewer than 100 atoms).^{8,9} Perusal of contemporary literature indicates that the data-driven machine learning (ML) models have achieved impressive success in predicting major products in reactions,^{10,11} often neglecting mechanistic details such as the movement of electron, identities of key intermediates, invoking catalyst participation, etc.^{12,13,14,15,16} High significance of CRM in a broad array of reactions of high practical value makes the development

of ML models for CRM prediction an important endeavor that can bridge the gap between heuristic approaches and automated learning.

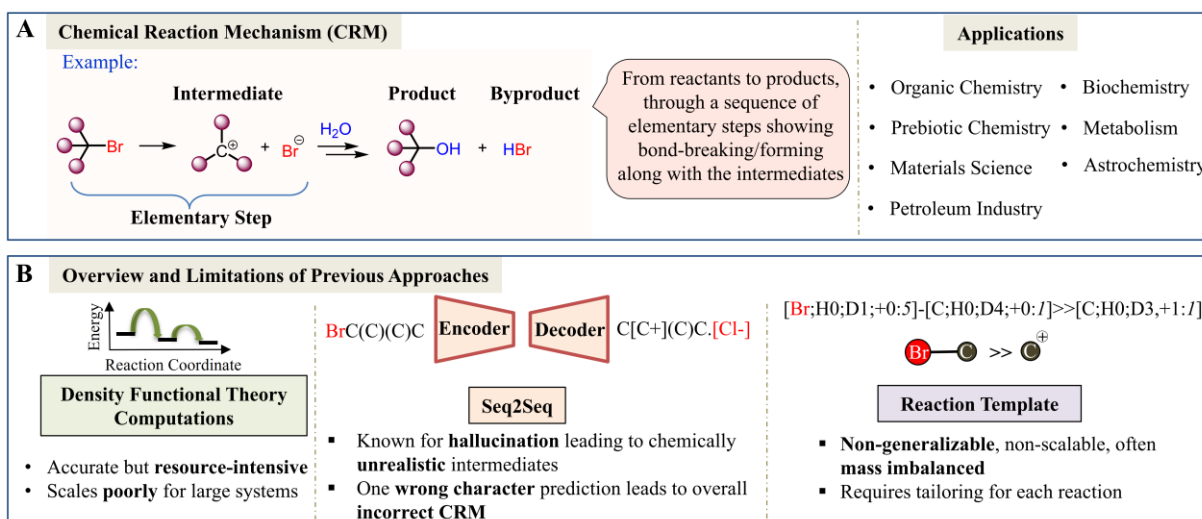


Fig. 1. (A) A representative elementary step involving a heterolytic bond breaking resulting in a carbocation in an S_N1 reaction mechanism. (B) An overview of previous approaches used in reaction mechanism prediction and their key limitations.

Recent efforts to integrate mechanistic details into chemical reaction datasets have led to some progress,^{17,18} but limitations remain. Although large reaction corpora like USPTO-Full¹⁹ and Pistachio provide extensive coverage of chemical reactions, they do not include mechanistic annotations. Early models were trained on textbook reactions to rank possible electron flows between donor and acceptor atoms/groups.^{20,21} A more recent dataset MechFinder, built on a subset of 31K reactions curated from the USPTO database, reports arrow-pushing diagrams but omits intermediate structures and excludes transition metal-catalyzed reactions. Given the industrial importance of transition metal catalysis, it is desirable to develop ML models suitable for such reactions as well.²² Further advancement in this area became possible by adapting end-to-end reaction prediction models to elementary steps, creating Graph2SMILES (G2S) based on the

Pistachio database.^{23,24} However, the curated dataset used in G2S model is not fully mass balanced and does not explicitly account for proton sources/sinks.

Sequence-to-sequence models that generate products character-by-character are prone to hallucinations, resulting in semantically invalid or chemically incorrect products. This limits their suitability for CRM tasks as it can adversely impact the accuracy and generalizability. We reasoned that bypassing SMILES-based generation could enable the model to focus on the underlying chemical reactivity. Graph-based models can serve as chemically intuitive alternatives,²⁵ and allow incorporation of attention mechanism facilitating the identification and prioritization of reactive atoms and bonds. Building on this rationale, we define the following objectives for this work.

- To create a reaction mechanism dataset ReactMech, that complements reaction databases like USPTO by providing mass-balanced elementary step mechanisms with explicit intermediates, which are otherwise absent in such datasets.
- To develop a robust and interpretable ML model for CRM prediction: We present DeepMech, the first model capable of predicting the complete reaction mechanism by learning template of mechanistic operations (TMOp). The model is desired to have (a) a strong generalization performance, in both in-distribution (ID) and out-of-distribution (OOD) reactions, (b) ability to identify side products and/or byproducts, which are important in reaction development, and (c) chemical interpretability for the predicted mechanisms.
- To explore prebiotic mechanisms: We extend our approach to prebiotic chemistry by curating a novel dataset, PrebioMech consisting of mechanistic pathways. Our DeepMech predicts plausible pathways toward higher-order amino acids and sugars, which are fundamental building blocks, respectively for proteins and carbohydrates in living systems, thus contribute toward understanding of chemical evolution in prebiotic environments.

Results and Discussions

A high-level overview of the DeepMech workflow is provided in Fig. 2, which contains the important building blocks A to F (Full details can be found in the Materials and methods section, SM section S1 & S2). We begin by creating a comprehensive reaction mechanism dataset, named as ReactMech. A representative example is shown in (A) to illustrate elementary step annotation, atom-mapping (B), and the corresponding SMILES representation (C). The data preprocessing (D) involves generation of labels in the form of reactive bonds and their corresponding TMOps. Each TMOp encodes three key components, such as (i) a generalized template (hereafter referred to as the ‘template’), (ii) the nature of the mechanistic operation (σ bond formation (σ -BF), σ bond breaking (σ -BB), π bond modification (π -BM), hydrogen atom exchange (HAX)), and (iii) the change in hydrogen count (ΔH) and formal charges (Δq) (sections B and C in Materials and methods).²⁶ The input reactant graph \mathbf{R} , and these labels are then used for training the DeepMech model (E) for two tasks. One is a binary classification task to predict the reactive and non-reactive bonds, and another multiclass classification of the identified reactive bonds into specific TMOps. In the next stage (F), the predicted bonds and TMOps are applied to \mathbf{R} , to generate products/intermediates, which are compared with the true products for accuracy evaluation. Building on this pipeline, DeepMech predicts intermediates and full CRMs directly from \mathbf{R} (see sections A and B in Materials and methods).

The model is evaluated based on the top- k accuracy, both at the elementary step level and the mechanism level predictions. While the former measures the accuracy of predictions on the most probable elementary step while the latter pertains to the complete CRM. We construct complete CRMs using a tailored beam search algorithm in conjunction with a separately trained AttentiveFP-based Reaction Classifier, serving as the stopping criterion for CRM completion (see

section D in Method). The DeepMech predictions are ranked using a top- k ranking of different likely CRMs given by the model. In the following sections, we highlight the key results and the significance of the DeepMech to different classes of reactions.

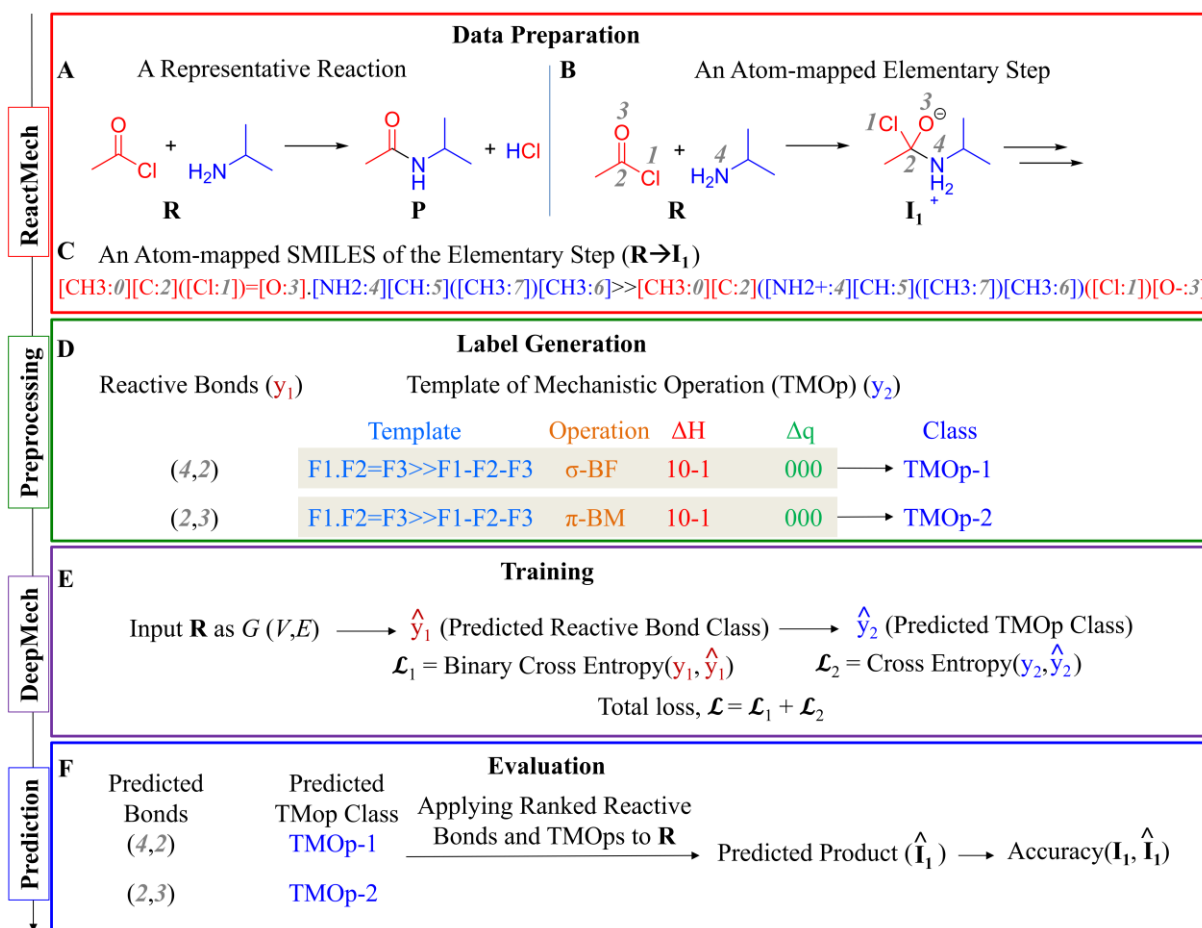


Fig. 2. The DeepMech workflow for the elementary step prediction, including (A,B,C) ReactMech dataset preparation, (D) preprocessing and label generation, (E) model training, and (F) product/intermediate prediction and evaluation.

Performance of DeepMech on Elementary Step Prediction

We evaluate the performance of DeepMech on elementary step predictions by using the top- k accuracy, obtained by comparing the SMILES strings of the predicted products with those of the true products. Top- k accuracy measures the fraction of predictions of the correct product in the

top- k predicted products ranked by the model. The top- k accuracies are averaged over five independent runs with distinct random train/validation/test splits. The standard deviation is provided to assess model stability. To compare the performance of our DeepMech model with the pseudo baselines, we re-trained two such models for elementary step prediction on our dataset.²⁷ One of these is a language-based transformer model and another a hybrid Graph2SMILES (G2S) model.²³ The transformer model considers the reaction mechanism prediction as a sequence-to-sequence task, translating the reactant SMILES into product SMILES.²⁸ In contrast, G2S encodes the reactants as graphs and decodes the products in the form of SMILES sequence. Both models were trained to predict the next intermediate or the final product.

As shown in Table 1, our model consistently outperforms the G2S and Transformer models, across all elementary step level top- k accuracy. The DeepMech achieves a top-1 accuracy of $98.98\pm 0.12\%$, surpassing both G2S ($98.00\pm 0.14\%$) and Transformer ($93.11\pm 0.27\%$). The performance gap becomes more pronounced when considering higher k values. In many realistic scenarios, the correct product may not always be ranked first, but could appear among the top few candidates. Therefore, the use of top- k metrics, such as top-2 or top-3, can provide a practically more useful application of the DeepMech model. Statistical analysis using a paired t -test confirms that the improvements over G2S are highly significant, with $p < 0.05$ across top-1, top-2, and top-3 accuracies ($p = 4.0\times 10^{-6}$, 1.6×10^{-6} , 1.1×10^{-6} respectively).

Table 1. Elementary Step Level Top- k Accuracy (%) Comparison of DeepMech and Baseline Models. Reported Values are Averaged over Five Independent Runs; Standard Deviations are Shown as \pm

Model	Top-1	Top-2	Top-3
DeepMech	98.98±0.12	99.41±0.09	99.46±0.08
G2S	98.00±0.14	98.57±0.11	98.64±0.10
Transformer	93.11±0.27	94.94±0.20	95.50±0.16

The relatively lower accuracy of the Transformer can be attributed to hallucination, which is a known issue with sequence-to-sequence architectures operating on SMILES representations (see SM section S12). In contrast, DeepMech, which operates on TMOp with explicit mechanistic semantics, avoids such inconsistencies.^{23,29} Motivated by the superior predictions of chemically valid elementary steps, we extended our model to complete CRM prediction tasks. It shall be noted that a chemical reaction could have several elementary steps leading to the major product as well as to byproducts.

Complete CRM Prediction in ID Scenario

In this section, we assess the model performance on complete CRM prediction within the ID settings.³⁰ Starting from a set of given reactants (**R**), the model predicts complete CRMs using the beam search strategy (Fig. 8). It is important to note that the mechanism level top-*k* accuracy is stringently defined for this evaluation. The predicted mechanism is considered correct, only if all the elementary steps match exactly to the corresponding steps in the ground truth CRM. Since a single mismatched prediction of any elementary step renders the entire prediction incorrect, we set the accuracy of such instances to zero.³¹

Table 2. Mechanism Level Top-*k* Accuracy (in %) for Full CRM Prediction in the ID Setting

Model	Top-1	Top-2	Top-3
DeepMech	95.94±0.21	96.13±0.16	96.70±0.09
G2S	93.52±0.67	93.56±0.65	93.70±0.70
Transformer	75.27±1.28	75.70±1.20	77.60±0.92

The top-*k* accuracies of our DeepMech model for CRM predictions can be compared with the other baseline models using the results provided in Table 2. Our model achieves a top-1 accuracy of 95.94±0.21%, significantly outperforming both the G2S (93.52±0.67%) and Transformer (75.27±1.28%). The performance margin widens further at higher *k* values. The paired *t*-test reveals that the performance improvements obtained with the DeepMech over the G2S

are statistically significant across top-1, top-2, and top-3 accuracies, with all corresponding p -values below 0.05 ($p = 1.1 \times 10^{-3}$, 8.7×10^{-4} , and 8.7×10^{-4} , respectively). Additionally, DeepMech demonstrates better robustness, as reflected in its lower standard deviation across runs. Although the training data for the baseline models differ slightly from that used for DeepMech, all these models are evaluated on the same test set to ensure fair comparison.²⁷ Once again, Transformer exhibits the weakest performance, consistent with our earlier observation in the case of elementary step predictions (Table 1). Following the promising performance of our DeepMech model, we became interested in visualizing the predictions to convey a chemically meaningful message. The predicted CRMs for different classes of representative reactions shown in Fig. 3 and 4 elucidate the formation of the desired products, byproducts, and side products,^{32,33} as well as the role of catalyst facilitating the bond-forming/breaking in multiple elementary steps of the reaction.³⁴

We present a representative example in Fig. 3 to illustrate the major steps involved in predicting one of the Pd-catalyzed BHA mechanisms. The DeepMech model is able to reconstruct the full catalytic cycle successfully, by predicting the key mechanistic steps such as the oxidative addition of Pd to the aryl halide ($\mathbf{R} \rightarrow \mathbf{I}_1^1$), coordination of the amine ($\mathbf{I}_1^1 \rightarrow \mathbf{I}_2^1$), deprotonation ($\mathbf{I}_2^1 \rightarrow \mathbf{I}_3^1$), and reductive elimination ($\mathbf{I}_3^1 \rightarrow \mathbf{P}$). Importantly, the model also predicts regeneration of the active catalyst correctly. In this example, these steps are predicted as the top-1 accuracy at the mechanism level top-1.

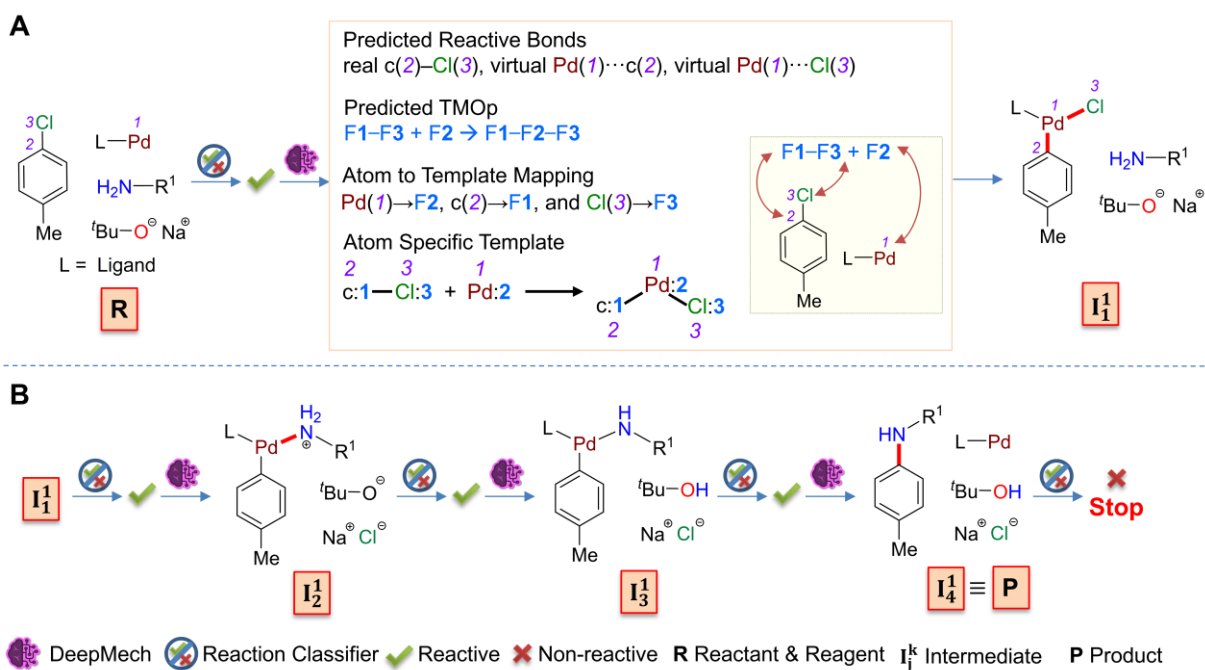


Fig. 3. A complete CRM prediction for a representative example of the Pd-catalyzed BHA reactions between p-chlorotoluene and alkyl amine in the ID setting. **(A)** The process begins with evaluation by the Reaction Classifier on the given set of reactants and reagents (together denoted as **R**). When the Reaction Classifier predicts **R** as reactive (✓), mechanistic inference is then carried out by the trained DeepMech model. In the first step, DeepMech identifies three reactive bonds (listed in the top row in the inset). It also predicts a TMOP for the given **R** (second row). Atom to template mapping is then performed to apply the predicted reactive atoms such as c(2), Cl(3), and Pd(1) to the template (third row). Substituting the atoms into the template provides the atom-specific mechanistic template (last row), which upon application to **R**, gives intermediate **I₁¹**. **(B)** The same procedure of predicting reactive bonds, TMOP, and atom to template mapping is followed to obtain the full CRM **R**→**I₁¹**→**I₂¹**→**I₃¹**→**P**.

In addition to yielding the desired products, a variety of side products are often likely to form during chemical reactions. The ability of our DeepMech model in predicting plausible side products can be appreciated using a representative aromatic nucleophilic substitution reaction

following an S_NAr mechanism as shown in Fig. 4A. The nucleophilic reactant in this case possesses two potentially reactive sites, an aliphatic amine and an aromatic amine. The mechanism level top-1 prediction by our model correctly identifies the aliphatic amine as the more nucleophilic center and yields the desired product. Interestingly, the top-2 prediction corresponds to an analogous mechanistic pathway initiated by the aryl amine, leading to a plausible side product. While such side products are often unreported in reaction datasets, their likely anticipation could be valuable for the design of reactions and the associated optimization efforts.

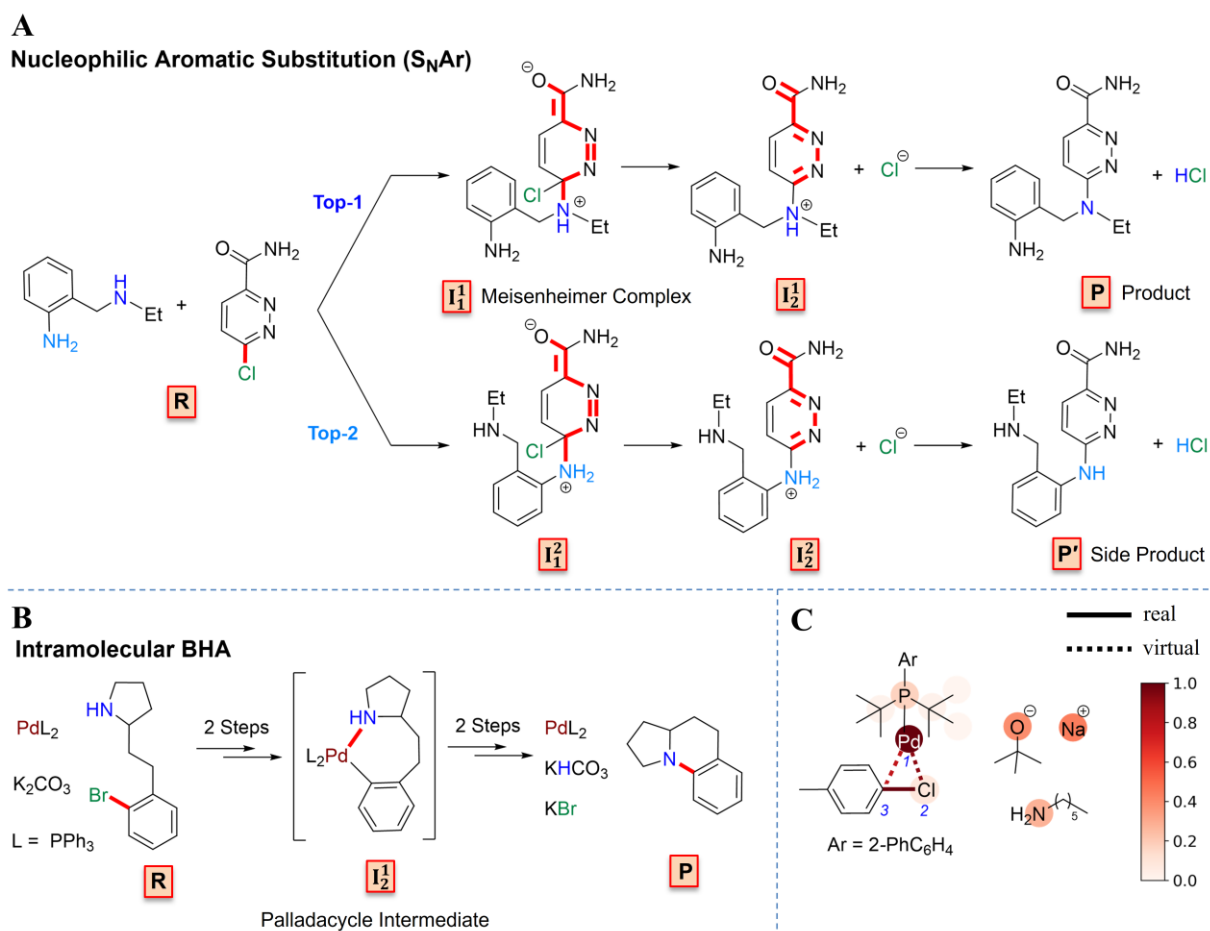


Fig. 4. Representative examples of full CRM prediction by the DeepMech model in the case of (A) an ID nucleophilic aromatic substitution reaction, and (B) an OOD intramolecular variant of the BHA reaction. (C) Visualization of atom and bond attentions in a representative oxidative

addition step involved in an ID BHA reaction. Atom attentions (top-10) are shown directly on molecular structures with colored circles, while selected bonds with higher attention are highlighted through color coding and increased line thickness. Deeper color intensity indicates higher attention.

In addition to predicting side products, another advantage of DeepMech is its ability to identify byproducts, often formed during the course of the main reaction.³⁵ In a representative reaction known as Appel reaction (fig. S8), wherein an alcohol gets converted to an alkyl halide by the action of triphenylphosphine and tetrahalomethane, DeepMech is found to predict each elementary step correctly along with the primary substitution product and identifies triphenylphosphine oxide as a byproduct. Chromatographic separation of this byproduct is known to be difficult due to its poor solubility in solvents like hexane and diethyl ether, even amounting to discarding it as a waste.^{36,37} Therefore, the ability of DeepMech in predicting byproducts as part of the overall mechanism could be of significant practical value to industries. Additionally, strategic removal or neutralization of byproducts at specific stages of the synthesis could as well be useful in shifting the equilibrium toward the desired product. Having obtained good accuracy in both the elementary step and full CRM predictions across a wide array of reactions in the ID setting, we considered more challenging OOD sets for evaluating the efficacy DeepMech.

Generalization to OOD Reactions

To evaluate generalization beyond the training distribution, we constructed an OOD dataset comprising CRMs from nucleophilic addition–elimination reactions involving amines and carbonyl compounds with different kinds of leaving groups. These compounds include acid halides, sulfonyl halides, anhydrides, haloformates, and carbamic halides. In addition, we have considered BHA reactions involving bidentate ligands and Ni catalysts, as well as its

intramolecular variants. These samples are structurally different from the Pd-catalyzed ID reactions with monodentate ligands. To enhance the chemical diversity in the OOD dataset, we have also included a new mechanistic class belonging to the C–O coupling reactions (see section S9 in the SM for details). The final OOD test set comprises of 9 mechanistically distinct classes and with a total of 3,778 CRMs.^{38,39,40,41,42} It shall be reckoned that the generalization capability of DeepMech, arises in part, from certain degree of underlying similarity in the elementary steps (TMOps) in the training set. A stricter OOD test would require reaction classes built from previously unseen TMOps. In such cases, the training set can be readily augmented with the new TMOps to enable the model to learn from the new data.⁴³

A perusal of the mechanism level top-1 accuracies of the OOD reaction classes, as compiled in Table 3, suggests that the DeepMech consistently outperforms both the G2S and Transformer, across nearly all categories of reactions. For instance, the reaction class involving amine and acid halide, an accuracy of $93.55\pm 0.72\%$ is much superior to $60.59\pm 4.77\%$ obtained with the G2S and to $16.41\pm 8.02\%$ with the Transformer. More importantly, both the baselines fail completely on reactions with anhydrides, whereas our model returns moderately good performance. Second, in the C–O coupling reaction, our model maintains a top-1 accuracy of $94.00\pm 2.31\%$. These results together highlight the ability of our DeepMech model to generalize well to reaction classes outside the training distribution. In scenarios where the top-1 accuracy is low, slightly relaxed criteria of using higher values of k led to significant improvements (see table S8 in SM). DeepMech achieves substantial improvements in each case, notably reaching $78.33\pm 3.11\%$ accuracy in the intramolecular BHA class, where both baseline models fail. These results strongly support the superior generalizability and robustness of DeepMech in handling complex and previously unseen chemical transformations.

Table 3. Mechanism Level Top-1 Accuracy (%) of Full CRM Prediction across OOD Reaction Classes

Reaction Class		DeepMech	G2S	Transformer
Amine +	acid halide	93.55±0.72	60.59±4.77	16.41±8.02
	sulfonyl halide	92.42±0.78	7.12±4.04	8.46±5.49
	anhydride	64.51±0.26	0.00±0.00	0.07±0.17
	haloformate	92.05±2.17	31.48±9.19	20.39±8.98
	carbamic halide	92.42±2.83	53.03±6.06	19.70±8.09
C–O coupling		94.00±2.31	16.00±4.00	0.00±0.00
BHA	intramolecular	78.33±3.11	0.00±0.00	0.0±0.00
	with bidentate ligand	99.90±0.22	0.00±0.00	0.00±0.00
	Ni-catalyzed	100.00±0.00	0.00±0.00	0.00±0.00

Another interesting application of DeepMech in predicting the elementary steps in a Pd-catalyzed intramolecular BHA reaction is shown in Fig. 4B, in which an aryl halide and amine moieties tethered within the same substrate leading to a cyclic product is considered. The mechanism is correctly predicted by the model, which begins with the oxidative addition of Pd to the C_{aryl}-Br bond, followed by intramolecular coordination of the pendant amine to the Pd center to form a palladacycle intermediate. Importantly, such palladacycles were not present in the training set. In the ensuing mechanistic steps, both deprotonation and reductive elimination is predicted in such a way that it leads to the desired benzo-fused indolizidine product, an important structural motif found in naturally occurring alkaloids⁴⁴ and regenerates the active catalyst. These examples collectively underscore the effectiveness of DeepMech in generalizing well beyond the reaction classes in the training set.

Consistently good performance of the DeepMech model on both ID and OOD deployments prompted us to wonder about possible factors contributing to its broad-spectrum capabilities. We attribute the absence of hallucination and model robustness to effective learning of the reactive bonds and classification of the reactive bonds into correct TMOps. This advantage enables accurate mechanistic predictions even in the case of highly diverse reactions. By focusing on

reactivity patterns rather than full molecule generation used in other baselines, DeepMech can minimize failures even when faced with unseen input reactants. Further, the integration of DeepMech with TMOp makes it less susceptible to hallucination, which otherwise could result in predicting a new atom that doesn't exist in the input molecules. All these are significant advantages of DeepMech, given that even one incorrect elementary step prediction can trigger generation a cascade wrong intermediates/product rendering the whole CRM invalid.

A few aspects of accuracy of DeepMech in full CRM prediction tasks invite a discussion. First, DeepMech performs exceedingly well in elementary step as well as multi-step mechanism predictions with the ID examples. A comparatively lower performance with the multi-step OOD case (Table 3) could arise from issues with the beam search and/or reaction classifier.⁴⁵ For instance, a full CRM prediction task is prone more errors as an incorrect prediction in any one elementary step during the beam search would render the whole mechanism invalid, even amounting to a zero in top-1 accuracy. Since the beam search classifier contains stopping as an outcome, a premature termination or prolongation of a predicted sequence beyond a chemically meaningful product could lead to unexpected errors. Although reliance on predefined TMOp might limit applications on new reactivity predictions, the ease of creation of a suitable TMOp for such scenarios can effectively resolve it.⁴¹ To probe into how DeepMech generalizes well across diverse reaction classes and to its potential interpretability, we have used graph attention visualization. In particular, in the following section, the attention on the reacting entities is analyzed toward developing an improved understanding of learnable aspects of DeepMech, when presented it with reaction mechanism datasets.

Attention Visualization

Given that DeepMech is constructed upon both atom- and bond-level attention mechanisms, as described in Fig. 4C, we have probed the attentive constituents to gather mechanistic insights and interpretability.⁴⁶ Interestingly, the atoms and bonds receiving high attention are found to be the ones expected to be the chemically reactive centers. This is illustrated using a representative oxidative addition step, characteristic of a BHA reaction, in Fig. 4C. The atom-level attention convincingly encompassed the primary reactive atoms (Pd and Cl) involved in this specific step, as well as secondary reactive atoms such as the nitrogen of the coupling partner. This suggests the model ability to recognize and weigh not only the immediate reaction site but also downstream reaction participants, thereby exhibiting enhanced interpretability spanning multiple stages. Importantly, adjacent atoms to the reactive centers (P and α -C of the ligand entity) also received moderate attention, which may reflect the influence of electronic and steric substituent effects, highlighting the model sensitivity to subtle, but chemically relevant, features. Additionally, the bond-level attention correctly focused on the reactive bonds in this elementary step, primarily highlighting the C–Cl bond undergoing cleavage and the Pd–C and Pd–Cl bonds being formed. Impressively, these bonds ranked among the top five most attentive, emphasizing their pivotal influence in this transformation. This marks the first instance, to the best of our knowledge, in which both real and virtual bonds have been jointly considered and substantially emphasized within an attention-based framework, representing a noteworthy advancement in the modeling of chemical reactivity (see section S8 in SM for more details).

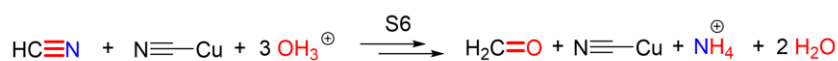
Application of DeepMech to Prebiotic Chemistry

To examine the applicability of our DeepMech model, we apply it to reaction mechanisms relevant to prebiotic chemistry, which concern the abiotic synthesis of biologically essential molecules

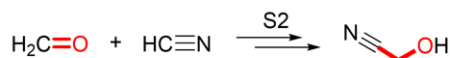
from simple primordial substrates. Elucidating the mechanistic pathways that lead to the formation of the basic building blocks, such as amino acids, sugars, and other biomolecular precursors from basic prebiotic inputs, such as H₂O, N₂, HCN, NH₃, and CH₄, is of fundamental importance to understanding the chemical origins of life. To systematically explore such chemical space, we followed the protocol outlined in the section ‘Dataset Preparation’ to generate a large-scale dataset of 30,787 elementary steps.⁴⁷ This dataset, which we refer to as PrebioMech, represents a diverse and chemically reasonable set of reaction mechanisms in line with prebiotic conditions (see section S10 in SM for further details).

A Reaction

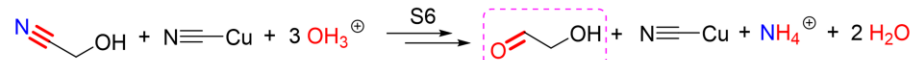
Formation of Aldehyde from Nitrile



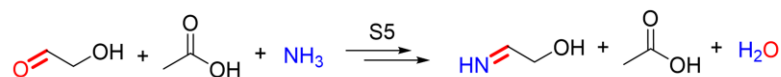
Addition of Cyanide to Carbonyl



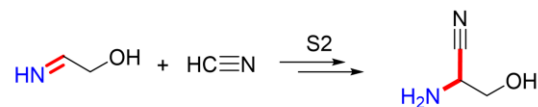
Formation of Aldehyde from Nitrile



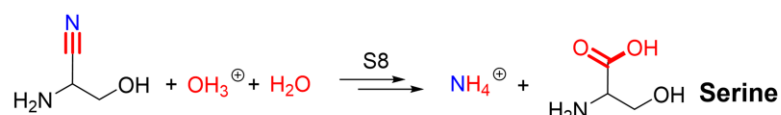
Formation of Imines



Addition of Cyanide to Imine

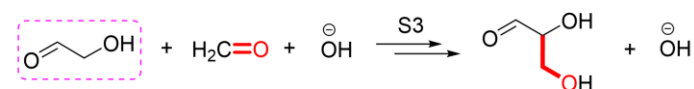


Nitrile Hydrolysis



B First three reactions follow the same predicted mechanistic pathway as in Serine synthesis

Aldol Addition



Aldol Addition

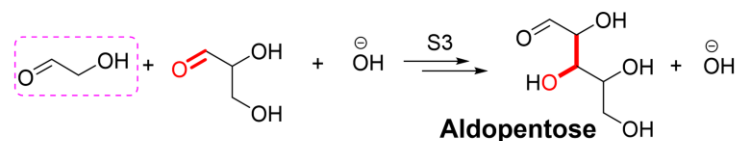


Fig. 5. Predicted mechanistic steps for the synthesis of (A) Serine (6 reactions) and (B) Aldopentose (5 reactions) using DeepMech starting from prebiotic compounds. Here, number of elementary steps in each transformation is denoted as S_n where $n=1,2,3, \dots,n$.

Using this dataset, we re-train the DeepMech model and evaluate its ability to predict mechanistic pathways leading to the formation of amino acids and other biologically relevant molecules. Remarkably, the model successfully reconstructs complete mechanistic routes for several amino acids. Fig. 5A illustrates the complete reaction network (see section S10 in SM for the associated predicted mechanisms) that leads to the formation of serine, a key naturally occurring α -amino acid. The mechanistic prediction of serine formation pathway uses formaldehyde, which in turn, is obtained from hydrogen cyanide (see first row in Fig. 5A). DeepMech reconstructs all the likely elementary steps. In the second row, the resulting formaldehyde reacts with HCN via two steps: a protonation followed by nucleophilic attack to yield an α -cyano alcohol. In the third row, this alcohol undergoes a series of mechanistic steps analogous to those in the initial formaldehyde formation, leading to the formation of an α -hydroxy aldehyde. In the fourth row, ammonia reacts with the α -hydroxy aldehyde to form the corresponding imine. Subsequently, in the fifth row, a second equivalent of hydrogen cyanide is added to the imine through a mechanism similar to that described in row two. Finally, the resulting 2-amino-3-hydroxypropanenitrile undergoes nitrile hydrolysis, a sequence comprising nine elementary steps, culminating in the formation of the amino acid serine (shown in the sixth row). The model accurately predicts all 29 elementary steps, validating the effectiveness of our TMOp based approach for reconstructing complete reaction mechanisms.

In addition to serine, DeepMech successfully predicts the formation of an important biologically relevant target molecule, specifically an aldopentose, as illustrated in Fig. 5B. The

initial three reaction steps leading to the formation of aldopentose are the same as those involved in serine biosynthesis. The resulting α -hydroxy aldehyde subsequently undergoes a base-catalyzed aldol addition with formaldehyde to yield an α,β -dihydroxy aldehyde. This aldehyde then participates in a second aldol addition with another molecule of α -hydroxy aldehyde, ultimately producing the aldopentose sugar. These results underscore the versatility and generalizability of the DeepMech framework that goes beyond the conventional reactions. More broadly, this demonstrates that our TMOp-based approach can be extended to other important areas such as astrochemistry, biochemical transformations, metabolic pathways, and petrochemical processes. As a future direction, we could continue integrating DeepMech with experiment or ab initio calculations to refine its fidelity to complex mechanistic problems.

Conclusions

We present DeepMech, a graph-based deep learning model for complete chemical reaction mechanism (CRM) prediction and ReactMech dataset containing mechanistic steps of a wide array of chemical reactions. Unlike sequence-to-sequence models that generate products of reactions by using a character-by-character approach, making them vulnerable to hallucinations, our DeepMech is designed to learn reactive bonds and template of mechanistic operations (TMOp). The integration of subgraph isomorphism, a reaction classifier as a stopping criterion, and a tailored beam search approach together is found to be effective in accurate identification of full and chemically plausible mechanistic pathways. Trained on the meticulously curated ReactMech dataset containing reactions from USPTO and transition metal catalysis, DeepMech achieves a high accuracy of $98.98\pm 0.12\%$ in elementary step predictions and $95.94\pm 0.21\%$ with in-distribution CRM predictions, outperforming pseudo baselines such as Graph2SMILES and Transformers. The generalizability of the DeepMech model became evident from the robust

performance with the out-of-distribution CRM prediction tasks, achieving superior accuracies than the baseline models. Moreover, DeepMech can identify potential side products and/or byproducts, which could be of importance to industrially important reactions. The core design components of DeepMech is built around the identification of reactive atoms and bonds involved in each elementary step, due to which the model offers mechanistic interpretability and insights consistent with chemical intuition. We could further showcase the broader applicability of DeepMech by successfully reconstructing multistep mechanisms relevant to prebiotic chemistry, starting from simpler precursors such as nitrogen, ammonia, methane and others, to important biological building blocks amino acid/sugars. In summary, DeepMech is a reliable, generalizable, and interpretable framework for CRM prediction that integrates data-driven modeling with mechanistic principles, which can be potentially extended to advanced predictive chemistry, reaction development and mechanism validation.

Materials and methods

We have organized the methods section in four major subsections to provide a concise detail of each of the distinct, but inter-dependent, building blocks in our workflow. First, steps involved in creating a multi-step reaction mechanism dataset (ReactMech) are described. Next, the key components in building our graph-based DL model (DeepMech) are presented. Subsequently, we describe how the prediction of reactive bonds and TMOps by DeepMech are used to infer the intermediate or product structures in elementary steps of chemical reactions. The utilization of the beam search algorithm for ranking top- k predicted mechanistic pathways is explained.

A. The Dataset: ReactMech

In this study, we use a subset of the reaction data extracted from the USPTO as compiled by Lowe.¹⁷ Given that this subset does not contain any transition metal catalyzed reactions, we

augment our dataset with 7 additional reaction classes to broaden the mechanistic coverage. Thus, our ReactMech dataset consists of 60 different reaction classes (see section S2 in SM) from the USPTO and 6 representative sets of transition metal catalyzed coupling reactions (Buchwald–Hartwig amination (BHA),⁴⁸ Suzuki–Miyaura,⁴⁹ Kumada,⁵⁰ Heck,⁵¹ relay-Heck,⁵² and C–H activation reactions).⁵³ In addition, the inclusion of Diels–Alder cycloaddition reactions⁵⁴ brings a desirable mechanistic diversity in the form of pericyclic reactions. Collectively, the ReactMech dataset provide 29,604 reactions belonging to 67 different reaction classes.⁵⁵ We utilized this dataset to create atom-mapped and mass-balanced full CRMs, providing a total of 104,964 elementary steps. To our knowledge, such a comprehensive mechanistic dataset is currently absent in literature that encompasses a broad range of reaction classes characterized by their underlying mechanisms.

We illustrate the key steps involved in the data preparation using Fig. 6. A simple reaction (Rxn:1, row-1) between acetyl chloride and isopropylamine leading to *N*-isopropylacetamide as the product is considered here. This reaction belongs to a widely found class of addition–elimination reaction exhibited by carbonyl derivatives. The domain knowledge and literature reports can help propose a plausible CRM, consisting of one or more elementary steps with relevant intermediates $\{\mathbf{I}_1, \mathbf{I}_2, \dots, \mathbf{I}_n\}$ with full mass balance at each such step (row-2). In every step, a few of the atoms undergo changes in their environment (e.g., charge, number of hydrogen atom, bonding). It is important to map the atoms of the reactants precisely to corresponding atoms in the products. Each of these atom mapped elementary step, leading to intermediates or products, constitutes an instance in the ReactMech dataset.

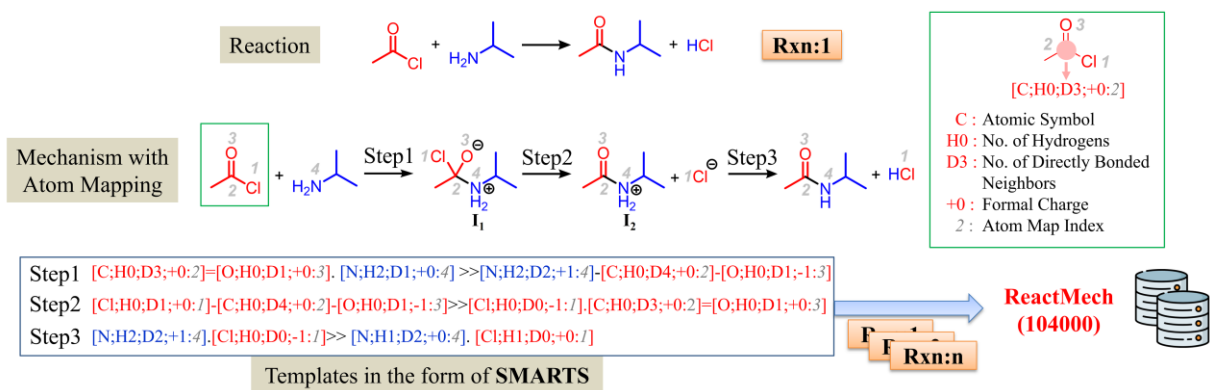


Fig. 6. An overview of the stepwise chemical reaction mechanism (CRM) generation to form ReactMech dataset for elementary steps. A chosen reaction (e.g., Rxn:1) is first subjected to annotation of mechanism and atom mapping. For each elementary step (e.g., Step1, Step2, and Step3), mechanistic templates in the form of SMARTS are extracted. These templates are then used to generate CRMs for other reactions (Rxn:2,...,Rxn:n) belonging to the same class. The resulting set of elementary steps collectively forms the ReactMech dataset. Shown in the inset is an example of a SMARTS pattern for a carbon atom in one of the substrates in Rxn:1.

Next, we developed an algorithm to automate the generation of atom mapped elementary steps for all the other reactions in the same class. From each atom mapped elementary step, the corresponding SMARTS-based template with full specification of the reactive atoms and bonds, is created as shown in row-3 of Fig. 6. The algorithm takes the initial reactant(s) and then applies a sequence of SMARTS-based templates iteratively i.e., the intermediates generated by a previous template serve as the input for the next template until the final product is obtained. Similarly, the remaining reactions (e.g. Rxn:2,...,Rxn:n) are passed through these templates to derive all the atom mapped elementary steps. For the reactions where the reactants couldn't be matched with any of the preset templates, we consider it as a failure mode and tackle them individually as follows. A template mismatch reaction is first subjected to a chemically meaningful mechanistic annotation

(row-2, Fig. 6), followed by atom mapping and then a new/modified template suitable for that reaction class is generated (See section S7 in the SM). This approach would readily facilitate inclusion of new reaction classes on which our algorithm can be applied to generate the corresponding reaction mechanism. Such modular operational advantage helps in expanding the scope of the ReactMech dataset for new reaction classes. The ReactMech, with 67 reaction classes and 29,604 reactions in it, gives a total of 104,964 elementary steps, providing a wide coverage of different chemical reactions.⁵⁶

B. The Model: DeepMech

The details of the DeepMech workflow for predicting elementary steps as well as full CRM are provided here.⁵⁷ As shown in Fig. 7A, the model operates on molecular graphs (G), which serve as a structured representation of the chemical species involved. Each graph encodes atoms as nodes (V) and bonds as edges (E), with initial atomic features h_u^0 derived from the Weave featurization strategy.⁵⁸ A Message Passing Neural Network (MPNN) is employed to update atomic features h_u , where each atom u receives messages from its neighbors v .⁵⁹ Through several message-passing steps, the atomic embeddings are iteratively refined to capture local structural information. Next, we apply a distance-aware Global Reactivity Attention (GRA) module, based on multi-head self-attention, on the MPNN-derived atomic embeddings to capture long-range dependencies.⁶⁰ This module integrates an Atom Distance Matrix (ADM), where each element $r_{u,v}$ denotes the topological distance (i.e., number of bonds) between atom pairs u and v .⁶¹ By incorporating these distance-aware relationships, the GRA module selectively attends to chemically relevant atom pairs, such as those involved in rings, aromatic systems, or functional groups, thereby enhancing the identification of potentially reactive sites.

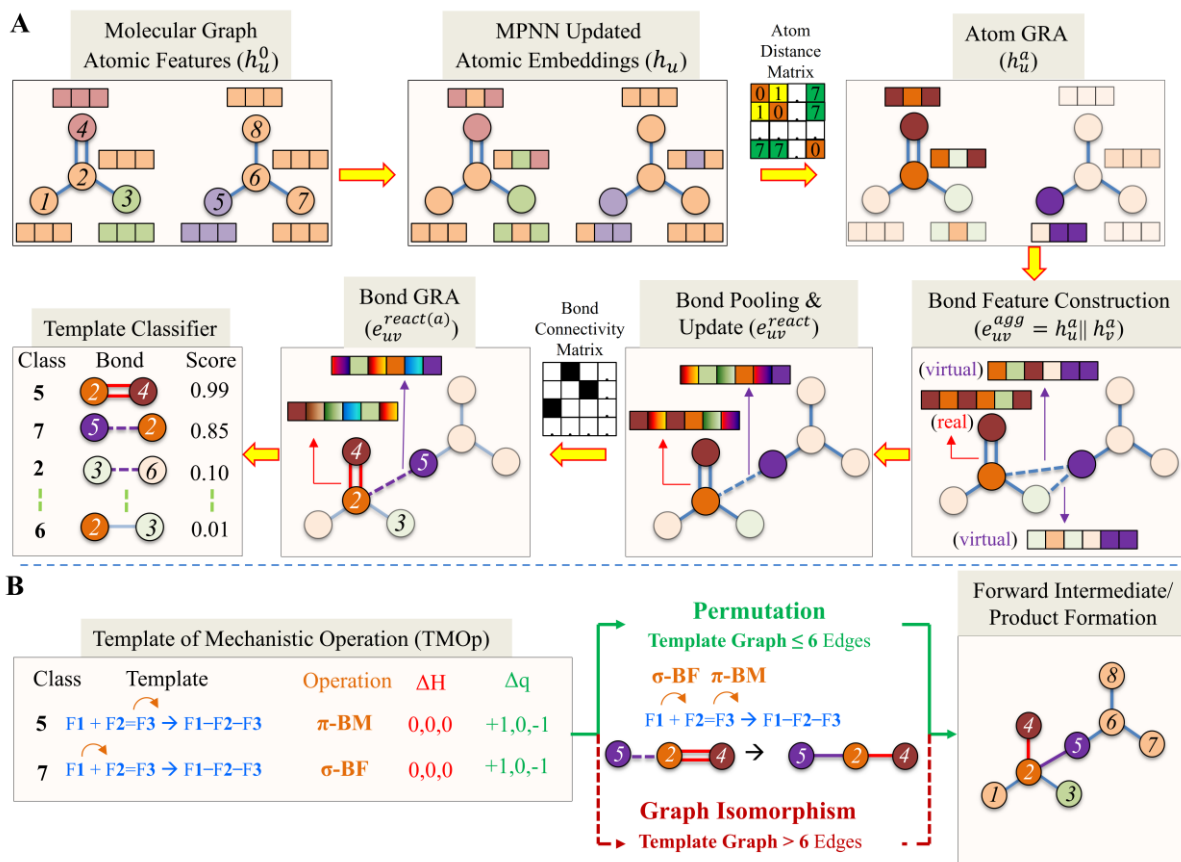


Fig. 7. Overview of the DeepMech workflow for prediction of elementary steps in chemical reaction mechanism. **(A)** In top right corner, the atoms with higher attention are shown with a deeper color while those with a lesser attention appear faded. In the second row, rightmost box shows a subset of real and virtual bonds for improved clarity. In the box denoted as Bond GRA (global reactivity attention), those bonds receiving higher attention are given different colors (red and violet for real and virtual bonds respectively) with a higher intensity, while those with lesser attention are shown faded. **(B)** An illustration of TMOp is given, where ΔH and Δq respectively denote the changes in the number of hydrogen atoms and formal charges. The actions such as σ bond formation (σ -BF), σ bond breaking (σ -BB), and π bond modification (π -BM) involved in TMOp are shown.

For each atom pair (u,v) , we construct a bond-level feature vector e_{uv}^{agg} by concatenating their refined atomic embeddings as shown in Fig. 7A (second row). This is done for both the real bonds, i.e., the edges present in the molecular graph, and the virtual bonds connecting atom pairs that are not directly bonded.⁶² The virtual bonds are shown using dashed lines in Fig. 7A. These virtual connections are designed to capture potential bond formation that is expected to occur during a chemical reaction, which facilitate the model to learn intermolecular interactions. To identify the top- k most reactive bonds e_{uv}^{react} , we apply a reactivity pooling strategy. Further, to account for the structural context and relational dependencies among the reactive bonds, an additional GRA module is introduced. This module operates on a Bond Connectivity Matrix, which encodes whether two bonds share a common atom, thereby indicating direct topological relationships within the molecular graph. For each pooled reactive bond, a multiclass classifier is trained to predict the probability distribution over a predefined set of 545 TMOps, which consider the changes in charge and number of hydrogen atoms.

A comparison between Fig. 6 and 7 brings out the advantage of our approach. The atom-specific template for Step 1 shown in the third row in Fig. 6, is only applicable to a nucleophilic addition of any primary amine on a carbonyl carbon. On the other hand, a template such as $F1.F2=F3 \gg F1-F2-F3$, can represent a general bond formation between **F1** and **F2** and a double bond breaking between **F2** and **F3**. Therefore, it can be applied to any other reaction with this kind of elementary step, such as a nucleophilic addition of an amine, alcohol, or thiol to double bonded subsystems such as a C=O in aldehydes, ketones, or other carbonyl derivatives encompassing a large group of reactions. Similarly, the subsystem could as well be C=C in alkenes, C=N in imines, and S=O in sulfonyl derivatives. This approach therefore provides significant advantages over the atom specific template-based methods, which rely on atom-specific constraints. Next, key feature

of TMOp is the inclusion of the operation type such as a σ bond formation (σ -BF), denoting the flow of electrons from an electron rich to electron poor atom/center, σ bond break (σ -BB), π bond modification (π -BM), and hydrogen atom exchange (HAX). Furthermore, the changes in the hydrogen count and formal charge are inherently taken into account in TMOp. Fig. 7B illustrates a TMOp consisting of two operations, a σ -BF (bond formation between F1 and F2) and a π -BM (conversion of a double bond to a single bond between F2 and F3) (see section S3 in SM for details). After the classification, TMOps and their associated pooled bonds are ranked by the corresponding probabilities, and the top-ranked ones are sequentially selected until their combined operations satisfy the corresponding TMOp. This TMOp is then applied on the identified reaction centers to generate the predicted structure, as detailed in the following section.

C. TMOp (Template of Mechanistic Operation) to Predicted Structure

To fit the predicted bond sets with the predicted TMOps, we implement a strategy based on the size of the template graph present within the TMOp. For template graph of ≤ 6 edges, we consider the full permutation space of the n predicted bonds to balance tractability and coverage. This permutation-based matching can be understood with the help of an illustrative example shown in Fig. 7B where the template graph has **(1,2)** and **(2,3)** as its two edges (Fig. 7B). Note that the numbers in bold font type denote numbering used in the template, while italic font represents the atom index in the predicted bonds such as (2,4), (3,6), and (2,5). Here, the task is to identify valid atom to template mapping that preserve the edge connectivity of the template. Since the predicted bonds are three and the template edges are two, we evaluate all ${}^3P_2 = 6$ permutations of the predicted bonds. These permutations can be aligned with the ordered nodes from the template graph. For example, under the mapping $\{1 \rightarrow 5, 2 \rightarrow 2, 3 \rightarrow 4\}$, the edges **(1,2)** and **(2,3)** get correctly mapped to the predicted bonds (5,2) and (2,4) respectively, which corresponds to one of the

permutations (middle inset in Fig. 7B). Here, **1** refers to **F1** in the template and **5** denote the predicted attentive atom. Similarly, mapping $\{2 \rightarrow 2, 3 \rightarrow 4\}$ respectively pertains to **F2** and atom **2** and **F3** and atom **4**. Thus, this permutation is considered a valid match, which will lead to the predicted structure. Conversely, an alternative permutation involving $(2,4)$ and $(3,6)$ as the predicted bonds will not lead to any valid mapping, rendering such permutations invalid as it fails to preserve connectivity.

While the above-mentioned approach can systematically explore the permutation space to identify structurally consistent mappings with small size graphs, it can become computationally intractable for larger graphs. Even in the case of a system with 12 predicted bonds and a template graph with $r = 7, 8, \text{ or } 9$ edges, the number of possible permutations become as large as 4M, 20M, and 80M, respectively. Thus, for graphs with more than 6 edges, we leverage subgraph isomorphism techniques to avoid the combinatorial explosion of permutations. The idea is to identify isomorphic subgraphs of the true structure from the predicted bonds.⁶³ Establishing these correct mappings between the predicted bonds and the template enables the derivation of the forward intermediate or product structure. Although this approach can predict the immediate next intermediate relevant to elementary step prediction, it does not provide the complete CRM. To achieve our objective of CRM prediction, we therefore implement a beam search algorithm designed to efficiently explore and rank multiple plausible mechanistic pathways.

D. Beam Search

DeepMech generates top- k predictions for a given input to construct a complete CRM using a tailored beam search algorithm in conjunction with a Reaction Classifier as shown in Fig. 8.

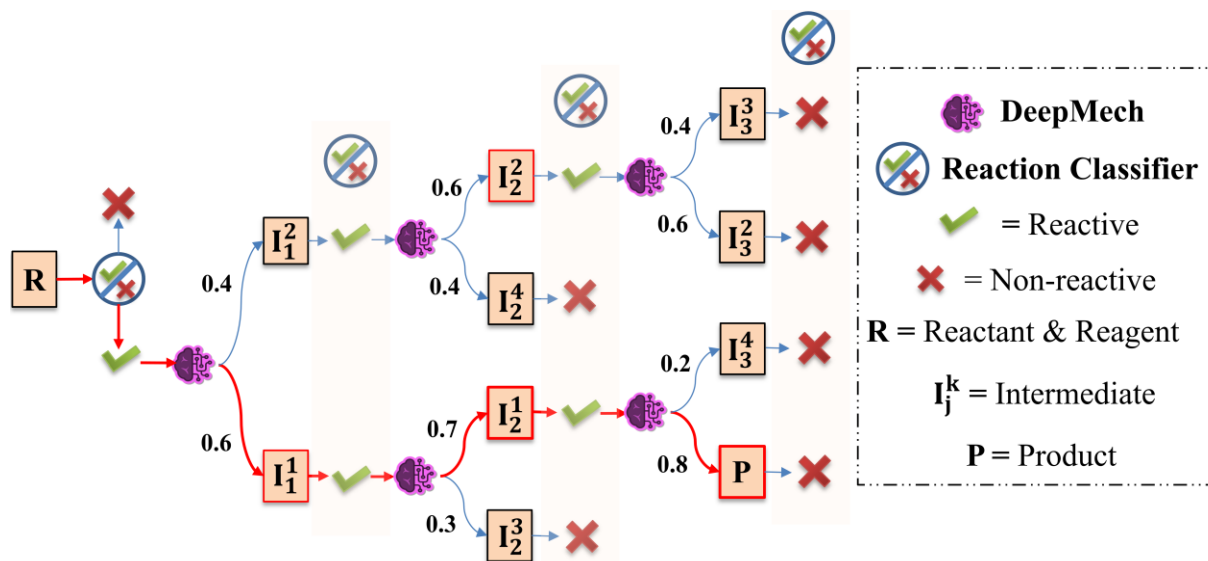


Fig. 8. Illustration of complete CRM prediction using the beam search algorithm.

Given a set of initial chemical entities (i.e., reactants, catalyst, and other reagents) as the input to the model, it is first evaluated by the AttentiveFP-based Reaction Classifier to verify whether a reaction is likely or not.⁶⁴ This classifier, which is trained to label the input as reactive or non-reactive, serves as a stopping criterion for the CRM generation if a given input is predicted as non-reactive, leading to a termination of the process at this very step (see section S5 in the SM for more details). Otherwise, the model proceeds to propose the top- k most probable next products, along with their associated probabilities. We apply domain-specific chemical heuristics to the top- k predictions to filter out chemically implausible products and to prioritize among predictions with comparable probabilities (see SM in section S5 for more details). Each product is then evaluated by the same Reaction Classifier to determine whether the predicted CRMs have reached completion (i.e., Reaction Classifier predicts it as non-reactive) or it should be further expanded. The CRMs deemed incomplete are expanded through additional predictions by the DeepMech model, with their cumulative log probabilities updated at each step. This process continues until all candidate CRMs are classified as complete or a predefined maximum depth (which is set to three in the illustration shown in Fig. 8) is reached. To prevent premature truncation or excessive

growth, we apply length normalization using a length-dependent factor α , which balances predicted CRMs probability against its length (i.e., $Normalized\ Score = (\log P(CRM))/(length)^\alpha$).

The resulting normalized scores are then used to rank the candidate CRMs, facilitating the selection of the top- k chemically plausible pathways.

Acknowledgements

We are thankful to Institution of Eminence (IoE) Data and Information Science computing facility for generous computational resources. M.D. acknowledges the Prime Minister's Research Fellowship.

Funding: not a funded project

Author contributions:

Conceptualization: M.D., A. H., M. B., R. B. S.

Methodology: M.D., A. H., M. B., R. B. S.

Investigation: M.D., A. H.

Visualization: M.D., A. H., M. B., R. B. S.

Supervision: M. B., R. B. S.

Writing – original draft: M.D., A. H.

Writing – review & editing: M.D., A. H., M. B., R. B. S.

Competing interests:

The other authors declare no competing interests.

References and Notes

1. K. R. Campos, P. J. Coleman, J. C. Alvarez, S. D. Dreher, R. M. Garbaccio, N. K. Terrett, R. D. Tillyer, M. D. Truppo, E. R. Parmee, The importance of synthetic chemistry in the pharmaceutical industry. *Science* **363**, 6424 (2019).

-
2. L. Jiang, E. A. Althoff, F. R. Clemente, L. Doyle, D. Röthlisberger, A. Zanghellini, J. L. Gallaher, J. L. Betker, F. Tanaka, C. F. Barbas 3rd, D. Hilvert, K. N. Houk, B. L. Stoddard, D. Baker, De novo computational design of retro-aldol enzymes. *Science* **319**, 1387–1391 (2008).
 3. D. E. Levy, *Arrow Pushing in Organic Chemistry: An Easy Approach to Understanding Reaction Mechanisms* (Wiley-Blackwell, Hoboken, NJ, 2008).
 4. A. L. Dewyer, A. J. Argüelles, P. M. Zimmerman, Methods for exploring reaction space in molecular systems. *Wiley Interdiscip. Rev. Comput. Mol. Sci.* **8**, e1354 (2018).
 5. E. Goldstein, B. Beno, K. N. Houk, Density functional theory prediction of the relative energies and isotope effects for the concerted and stepwise mechanisms of the Diels–Alder reaction of butadiene and ethylene. *J. Am. Chem. Soc.* **118**, 6036–6043 (1996).
 6. R. B. Sunoj, Transition state models for understanding the origin of chiral induction in asymmetric catalysis. *Acc. Chem. Res.* **49**, 1019–1028 (2016).
 7. S. Habershon, Automated prediction of catalytic mechanism and rate law using graph-based reaction path sampling. *J. Chem. Theory Comput.* **12**, 1786–1798 (2016).
 8. M. Anand, R. B. Sunoj, H. F. Schaefer III, Non-innocent additives in a palladium(II)-catalyzed C–H bond activation reaction: Insights into multimetallic active catalysts. *J. Am. Chem. Soc.* **136**, 5535–5538 (2014).
 9. S. Bahmanyar, K. N. Houk, H. J. Martin, B. List, Quantum mechanical predictions of the stereoselectivities of proline-catalyzed asymmetric intermolecular aldol reactions. *J. Am. Chem. Soc.* **125**, 2475–2479 (2003).
 10. L. M. Sigmund, M. Assante, M. J. Johansson, P.-O. Norrby, K. Jorner, M. Kabeshov, Computational tools for the prediction of site- and regioselectivity of organic reactions. *Chem. Sci.* **16**, 5383–5412 (2025).

-
11. M. Das, A. Ghosh, R. B. Sunoj, Advances in machine learning with chemical language models in molecular property and reaction outcome predictions. *J. Comput. Chem.* **45**, 1160–1176 (2024).
 12. J. Burés, I. Larrosa, Organic reaction mechanism classification using machine learning. *Nature* **613**, 689–695 (2023).
 13. C. W. Coley, R. Barzilay, T. S. Jaakkola, W. H. Green, K. F. Jensen, Prediction of organic reaction outcomes using machine learning. *ACS Cent. Sci.* **3**, 434–443 (2017).
 14. P. Schwaller, T. Laino, T. Gaudin, P. Bolgar, C. A. Hunter, C. Bekas, A. A. Lee, Molecular transformer: A model for uncertainty-calibrated chemical reaction prediction. *ACS Cent. Sci.* **5**, 1572–1583 (2019).
 15. M. H. S. Segler, M. Preuss, M. P. Waller, Planning chemical syntheses with deep neural networks and symbolic AI. *Nature* **555**, 604–610 (2018).
 16. J. Bradshaw, M. J. Kusner, B. Paige, M. H. S. Segler, J. M. Hernández-Lobato, A generative model for electron paths. *arXiv* (2018). <https://doi.org/10.48550/arXiv.1805.10970>
 17. J. F. Joung, M. H. Fong, N. Casetti, J. P. Liles, N. S. Dassanayake, C. W. Coley, Electron flow matching for generative reaction mechanism prediction. *Nature* (2025). <https://doi.org/10.1038/s41586-025-09426-9>.
 18. S. Chen, K. S. Park, T. Kim, S. Han, Y. Jung, Predicting chemical reaction outcomes based on electron movements using machine learning. *arXiv* (2025). <https://arxiv.org/abs/2503.10197>.
 19. D. M. Lowe, Extraction of chemical structures and reactions from the literature. Ph.D. thesis, University of Cambridge (2012).
 20. J. H. Chen, P. Baldi, No electron left behind: A rule-based expert system to predict chemical reactions and reaction mechanisms. *J. Chem. Inf. Model.* **49**, 2034–2043 (2009).

-
21. M. A. Kayala, P. Baldi, ReactionPredictor: Prediction of complex chemical reactions at the mechanistic level using machine learning. *J. Chem. Inf. Model.* **52**, 2526–2540 (2012).
22. S. Chen, R. Babazade, T. Kim, S. Han, Y. Jung, A large-scale reaction dataset of mechanistic pathways of organic reactions. *Sci. Data* **11**, 863 (2024).
23. J.F. Joung, M.H. Fong, J. Roh, Z. Tu, J. Bradshaw, C.W. Coley, Reproducing reaction mechanisms with machine-learning models trained on a large-scale mechanistic dataset. *Angew. Chem. Int. Ed.* **63**, e202411296 (2024).
24. Z. Tu, C.W. Coley, Permutation invariant graph-to-sequence model for template-free retrosynthesis and reaction prediction. *J. Chem. Inf. Model.* **62**, 3503–3513 (2022).
25. A. Hoque, M. Das, M. Baranwal, R.B. Sunoj, ReactAIvate: A deep learning approach to predicting reaction mechanisms and unmasking reactivity hotspots. *European Conference in Artificial Intelligence* **392**, 2645–2652 (2024).
26. Examples of various TMOps are shown in the section S3 of SM.
27. It is important to note that the training dataset used for the DeepMech differs slightly from that employed in the case of the G2S and Transformer pseudo baseline models. Specifically, the baseline models are trained on a mildly modified dataset that also includes a ‘no-reaction’ class, wherein the reactants and products are identical, implying no net reaction. In these models, there is no dedicated Reaction Classifier to determine termination; instead, if the model predicts the same SMILES string as the input **R**, it is treated as a signal to stop the prediction process. In contrast, DeepMech excludes such no-reaction cases from its training set and instead uses a Reaction Classifier to determine reactivity. Despite these differences in the training data and stopping criteria, all models are evaluated on the same test set to ensure a fair and consistent

comparison of their predictive performance. The hyperparameter settings used to train these baseline models are described in section S11 of the SM.

28. I. V. Tetko, P. Karpov, R. Van Deursen, G. Godin, State-of-the-art augmented NLP transformer models for direct and single-step retrosynthesis. *Nat. Commun.* **11**, 5575 (2020).

29. Chen S, Jung Y. Assessing the extrapolation capability of template-free retrosynthesis models. *arXiv* (2024). <https://doi.org/10.48550/arXiv.2403.03960>

30. To construct the ID dataset, we use a stratified random sampling based on the number of reactions in a given reaction class, spread across all 67 reaction classes to ensure a balanced distribution (see section A in Method). Specifically, number of samples drawn from an individual class are as follows; for reaction classes with ≤ 20 CRMs in them, no samples are taken, whereas those with 21–200 CRMs contributes 1–5 random samples. We sample 10% from those classes with >200 CRMs, together providing us with an ID dataset consisting of 2751 CRMs.

31. Details of how the mechanism-level top- k is calculated, along with an illustrative example, can be found in section S5 in the SM.

32. A byproduct is a compound produced as a direct consequence of the main reaction pathway and appears in the stoichiometrically balanced chemical equation. A side product, on the other hand, refers to those compounds formed through alternative or competing side reactions.

33. W. Watson On byproducts and side products. *Org. Process Res. Dev.* **16**, 1877–1877 (2012).

34. Additional examples of ID-CRM prediction by DeepMech are available in section S9 of the SM.

35. A. I. McKay, W. A. O. Altalhi, L. E. McInnes, M. L. Czyz, A. J. Canty, P. S. Donnelly, R. A. J. O’Hair, Identification of the side products that diminish the yields of the monoamidated product

in metal-catalyzed C–H amidation of 2-phenylpyridine with arylisocyanates. *J. Org. Chem.* **85**, 2680–2687 (2020).

36. The mechanism begins with a nucleophilic attack by triphenylphosphine on the C–Br bond of tetrabromomethane, generating a phosphonium halide cation with a new P–Br bond and a tribromomethyl carbanion. The latter abstracts a proton from the alcohol substrate, forming the corresponding alkoxide. The alkoxide subsequently attacks the phosphonium species, displacing a halide to yield an oxyphosphonium intermediate (see section S9 in SM for all the intermediates).

37. H. A. van Kalker, F. L. van Delft, F. P. J. T. Rutjes, Organophosphorus catalysis to bypass phosphine oxide waste, *ChemSusChem* **6**, 1615–1624 (2013).

38. H. Zhang, P. Ruiz-Castillo, S. L. Buchwald, Palladium-catalyzed C–O cross-coupling of primary alcohols. *Org. Lett.* **20**, 1580–1583 (2018).

39. J. P. Wolfe, R. A. Rennels, S. L. Buchwald, Intramolecular palladium-catalyzed aryl amination and aryl amidation. *Tetrahedron* **52**, 7525–7546 (1996).

40. M. Mari, F. Bartoccini, G. Piersanti, Synthesis of (–)-*epi*-indolactam V by an intramolecular Buchwald–Hartwig C–N coupling cyclization reaction. *J. Org. Chem.* **78**, 7727–7734 (2013).

41. J. Mao, J. Zhang, S. Zhang, P. J. Walsh, NIXANTPHOS: a highly active ligand for palladium-catalyzed Buchwald–Hartwig amination of unactivated aryl chlorides. *Dalton Trans.* **47**, 8690–8696 (2018).

42. C. M. Lavoie, M. Stradiotto, Bisphosphines: a prominent ancillary ligand class for application in nickel-catalyzed C–N cross-coupling. *ACS Catal.* **8**, 7228–7250 (2018).

43. A step-by-step procedure for incorporating any new TMOp as desired by a prospective user of our model can be found in section S7 of the SM. A full list of TMOps is provided in our Github repository.

-
44. D. L. Comins, K. Higuchi, Synthesis of the benzo-fused indolizidine alkaloid mimics, *Beilstein J. Org. Chem.* **3**, 42 (2007).
45. See section S5 in the SM that demonstrates how an incorrect prediction by the Reaction Classifier at an elementary step in the CRM sequence can lead to an erroneous CRM outcome.
46. Simultaneous removal of atom level and bond level attention modules resulted in a reduction of the mechanism-level top-1 accuracy from 95.85% to 86.34% for the ID CRM prediction tasks, suggesting the importance of attention modules. See table S6 in the SM for additional details.
47. A. Wolos, R. Roszak, A. Zadło-Dobrowolska, W. Beker, B. Mikulak-Klucznik, G. Spolnik, M. Dygas, S. Szymkuc, B. A. Grzybowski, Synthetic connectivity, emergence, and self-regeneration in the network of prebiotic chemistry. *Science* **369**, eaaw1955 (2020).
48. P. Ruiz-Castillo, S. L. Buchwald, Applications of palladium-catalyzed C–N cross-coupling reactions. *Chem. Rev.* **116**, 12564–12649 (2016).
49. I. P. Beletskaya, F. Alonso, V. Tyurin, The Suzuki–Miyaura reaction after the Nobel Prize. *Coord. Chem. Rev.* **385**, 137–173 (2019).
50. L. Ackermann, A. Althammer, Air-stable PinP(O)H as preligand for palladium-catalyzed Kumada couplings of unactivated tosylates. *Org. Lett.* **8**, 3457–3460 (2006).
51. W. Cabri, I. Candiani, Recent developments and new perspectives in the Heck reaction. *Acc. Chem. Res.* **28**, 2–7 (1995).
52. E. W. Werner, T.-S. Mei, A. J. Burckle, M. S. Sigman, Enantioselective Heck arylations of acyclic alkenyl alcohols using a redox-relay strategy. *Science* **338**, 1455–1458 (2012).
53. D.-H. Wang, X.-S. Hao, D.-F. Wu, J.-Q. Yu, Palladium-catalyzed oxidation of Boc-protected N-methylamines with IOAc as the oxidant: a Boc-directed sp³ C–H bond activation. *Org. Lett.* **8**, 3387–3390 (2006).

-
54. C. C. Lam, J. M. Goodman, Every atom counts: predicting sites of reaction based on chemistry within two bonds. *Digital Discovery* **3**, 1878–1888 (2024).
55. See section S2 of the SM that provides a comprehensive overview of reaction class distributions and diversity, highlighting the frequency of various classes such as DCC-condensation, nucleophilic substitution, Boc deprotection, reductive amination, and so on.
56. See section S7 of the SM where we illustrate how to include any new class of reaction as desired by a reader/user of this algorithm.
57. The full description of the building blocks and training details of the DeepMech are provided in sections S1, S5, and S6 in the SM.
58. S. Kearnes, K. McCloskey, M. Berndl, V. Pande, P. Riley, Molecular graph convolutions: moving beyond fingerprints. *J. Comput. Aided Mol. Des.* **30**, 595–608 (2016).
59. Gilmer, J.; Schoenholz, S. S.; Riley, P. F.; Vinyals, O.; Dahl, G. E. Neural message passing for quantum chemistry. *International Conference on Machine Learning* **2017**, 1263-1272. J. Gilmer, S. S. Schoenholz, P. F. Riley, O. Vinyals, G. E. Dahl, Neural message passing for quantum chemistry. *International Conference on Machine Learning* **70**, 1263–1272 (2017).
60. A. Vaswani, N. Shazeer, N. Parmar, J. Uszkoreit, L. Jones, A. N. Gomez, Ł. Kaiser, I. Polosukhin, Attention is all you need. *Advances in Neural Information Processing Systems* **30**, (2017).
61. In our approach, atom pair distances $r_{u,v}$ are discretized such that they equal the actual topological distance if $r_{u,v} \leq 5$, are set to 6 if the atoms are more than five bonds apart but belong to the same molecule, and set to 7 if the atoms are in different molecules.
62. S. Chen, Y. Jung, A generalized-template-based graph neural network for accurate organic reactivity prediction. *Nat. Mach. Intell.* **4**, 772–780 (2022).

63. A detailed discussion on the subgraph isomorphism is provided in section S5 of SM.

64. Z. Xiong, D. Wang, X. Liu, F. Zhong, X. Wan, X. Li, Z. Li, X. Luo, K. Chen, H. Jiang, M. Zheng, Pushing the boundaries of molecular representation for drug discovery with the graph attention mechanism. *J. Med. Chem.* **63**, 8749–8760 (2019).